A Hybrid Analytical-Numerical Approach for the Analysis of Salient-Pole Synchronous Generators with a Symmetrical Damper Cage

Stefano Nuzzo[1], Paolo Bolognesi[2], Michael Galea[1], Chris Gerada[1,3]
[1]Power Electronics, Machines and Control Group, University of Nottingham, Nottingham, UK, stefano.nuzzo@nottingham.ac.uk
[2]Electrical Machines, Power Electronics and Drives Group, University of Pisa, Pisa, Italy, p.bolognesi@ieee.com
[3]Power Electronics, Machines and Control Group, University of Nottingham Ningbo, Ningbo, China.

***Abstract*— The equivalent circuit approach has been widely exploited for the theoretical analysis of electromagnetic devices. However, in the field of classical wound-field synchronous generators, the presence of the damper cage complicates the analysis of such devices and the accurate prediction of the inherent induced currents is still matter of ongoing research. 12Focus is given to the accurate prediction of the no-load voltage waveform, by implementing a hybrid analytical-numerical model for a specific alternator.**

Keywords—Analytical Modeling, Synchronous Generators, Damper Cage, Equivalent Circuits

I. INTRODUCTION

Although wound-field synchronous generators (SGs) have been extensively studied over the years, the design and analysis of such machines is presently attracting attention again due to the ever-increasing power quality and efficiency requirements [1] and the improvements in the potential of the analysis tools available, such as powerful computing and accurate modelling resources. In this context, particular focus has recently been given to the damper winding usually embedded in the rotor of salient-pole SGs. In fact, although this additional winding is usually designed to improve the power system stability [2], it also affects the machine behaviour under different operating conditions, including steady-state. In fact, additional currents are induced and Joule losses are then also produced in the damper winding in any working condition, including no-load, due to the presence of parasitic harmonics in the airgap flux density [3]. These harmonics are mainly due to the tooth ripple, inherently accentuated in machines featuring an open slot structure, and to the armature reaction magneto-motive force, which causes parasitic effects when currents flow in the stator windings. A comprehensive picture of the concepts behind these parasitic effects as well as of the reasons for providing a damper cage in salient-pole SGs are provided in [4].

Whilst traditionally the damper cage design was approached by combining empirical considerations and classical *d-q* analysis based on sinusoidal approximation [5], more accurate techniques [6] have been recently proposed to predict the induced currents even under normal operating conditions, since the effects of such secondary phenomenon are often less negligible than traditionally assumed [4]. In particular, permeance models have been presented in [7] and [8], where the work was mainly aimed at evaluating the airgap flux density through a Fourier series decomposition. Aiming to the same purposes, an innovative numerical integration method has been proposed in [3]. With the recent advancements in the computational capabilities, accurate numerical methods are more and more used to analyse SGs taking into account the damper cage. In fact, different configurations of this additional rotor winding have been investigated in [9], where a sensitivity analysis was carried out to understand its behaviour under steady state and transient conditions. Finally, particular focus has been recently given to the impact that this winding has on the quality of the output voltage waveform [10]. In [4], an unconventionally displaced damper winding has been proposed for such purposes, while trying to minimise the ohmic losses associated with it.

This paper therefore deals with the implementation of a semi-analytical modelling approach for SGs, based on a generalized model for electromagnetic devices which is properly adapted to a specific machine. Particular attention is devoted to the damper cage, where appropriate assumptions allow for a reduction in the number of electromagnetic equations to be considered. Such model is then used to predict the open-circuit voltage waveform, considering in particular an industrial medium-power SG as a case study, whose main characteristics are listed in sec. I.A. The obtained results are finally compared to the data provided by a corresponding finite-element (FE) analysis of the machine: the very good matching achieved proves the validity of the proposed method.

A. Case study

All of the numerical quantities and graphical examples reported in this paper are referred to an industrial 3-phase alternator featuring 4 poles, 48 stator slots, with a rated power of 400*kVA* and a rated voltage of 400*V*, 50*Hz* achieved with Y-connection of armature phases. Such machine is equipped with a damper cage composed of 6 aluminium bars per pole, which are symmetrically located in the same positions around the central axes of the poles. A 2-D cross section of the magnetic core of such SG is shown Fig. 1. The bars of the damper cage

978-1-5090-4281-4/17/$31.00 ©2017 IEEE

are connected at each side by aluminium press-plates, which basically reproduce the rotor laminations shape with a larger thickness.

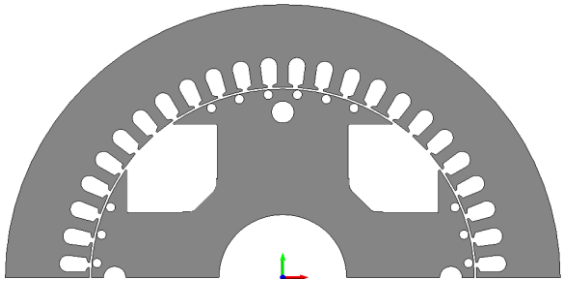

Fig.1. 2-D half-view of the core of the SG considered.as case study

II. Analytical Model

The equivalent circuit methodology has been widely investigated in literature, with the aim of analysing electromagnetic devices and more specifically rotating electrical machines. However, as recalled in Section I, the damper cage modelling and analysis still represents a challenge for SGs designers. A general model valid for any class of devices is then used for such purpose. The basic structure of the proposed analytical model is introduced and presented in [11]. However, updates and variations are investigated in this work.

A. Model Introduction and Main Assumptions

In order to set the context of the scheme, the main introductory assumptions are defined as follows:

- A main region, corresponding to the axial portion of the machine delimited by the magnetic cores, can be defined and differentiated from a secondary region, mainly involving the phenomena occurring in the end parts of the windings.
- Assuming that the shape of the magnetic cores and of the windings can be generated by straight extrusion along the machine axis, a 2-D approximation of the field map can be considered for deriving the general model.
- It is assumed that the ferromagnetic materials feature a sufficiently high permeability to permit neglecting the m.m.f. drop inside the cores with respect to the m.m.f. across the airgap.
- The phenomena related to hysteresis and eddy currents in the magnetic cores are neglected.
- The mutual influence between the main field lines and the secondary lines (representing the leakage fluxes) can be neglected, permitting to separately analyse such phenomena.
- The shape of the main flux lines in the airgap is assumed to be mainly determined by the profiles of the magnetic cores and by the rotor position, meaning that the dependency on the currents is neglected.
- The variation of magnetic field intensity along the portions of field lines in the main airgap is considered to be small, permitting to focus on the average value and on its variation along the tangential direction.

Although the basic, general framework of the model proposed in [11] is maintained for the analysis of the considered machine, it is clear that some adaptions and more assumptions need to be introduced for the sake of this study. In particular, as the main aim of the paper is that of estimating the no-load voltage waveform, it is necessary to introduce in the model the effects of the stator slot openings, as the related harmonics can play a very important role in determining the actual waveform of the output voltage. In other words, the stator slot openings cannot be neglected as in [11]. As a first approximation, their equivalent profile is represented by a trapezoidal variation of the inner radius of the stator core vs. angular location, assuming the same slot opening width *c* of the real laminations and considering as characteristic parameters only the depth *a* and the width *b* of the ramp. Referring for example to the considered case study, in Fig. 2 the trapezoidal approximation and a schematic representation of the original profile are sketched, highlighting the characteristic parameters being considered.

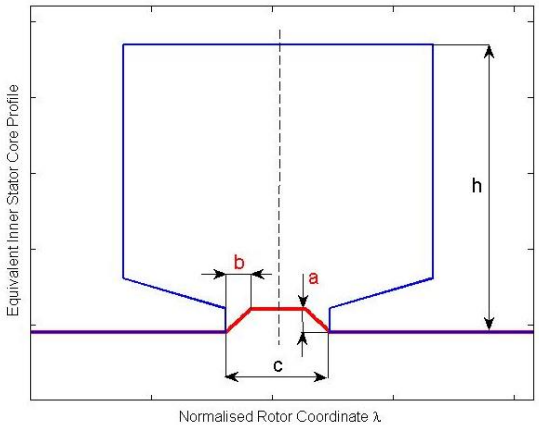

Fig.1. Representation of the actual (simplified) and equivalent inner stator profile.

The values of the equivalent parameters characterizing the slots are intended to be determined by means of a tuning procedure, carried out by comparing the results from the simplified model to the ones obtained by means of a 2-D electromagnetic FE model of the machine, as discussed in-depth in Sections III and IV.

Having recalled and updated the introductory aspects of the proposed analytical approach, it is now possible to proceed with the description of the model and with the definition of the main functions necessary to solve the electromagnetic problem.

B. Model Description

The vector voltage equation related to the equivalent circuit of a generic electrical machine is shown in (1), where the

hypothesis of linear characteristics for all of the magnetic materials is assumed.

$$\bar{v}(t) = R \cdot \bar{i}(t) + \overline{M}(\alpha(t), \bar{i}(t)) \cdot \frac{d\,\alpha(t)}{dt} + L(\alpha(t)) \cdot \frac{d\,\bar{i}(t)}{dt} \qquad (1)$$

In (1), the vector $\bar{i}$ is composed by the currents entering the machine phases (in broad sense, i.e. also including rotor circuits), α is the angular position of rotor vs. stator, while the matrices R and $L(\alpha)$ represent the resistances and inductances characterising the machine, respectively. The quantity $\overline{M}(\alpha, \bar{i})$ in (1) is the motional coefficients vector, which is obtained by derivation of the flux linkage vector with respect to the variable α, resulting in the expression given in (2).

$$\overline{M}(\alpha(t), \bar{i}(t)) \cdot = \left.\frac{\partial\, L(\alpha)}{\partial\, \alpha}\right|_{\alpha(t)} \cdot \bar{i}(t) \qquad (2)$$

By examining (1) and (2), it clearly emerges that the inductance matrix function $L(\alpha)$ plays a key role in the electromagnetic behaviour of the machine. Considering that the assumptions introduced in Section II.A match the hypotheses of the general analysis developed in [11], an approximated analytical expression of $L(\alpha)$ referred to the main flux tubes (i.e. those crossing the main airgap and contributing to the electromechanical energy transformation) can be obtained in the following general form:

$$L(\alpha) = l \cdot \int_0^1 \mu_E(\lambda, \alpha) \cdot \overline{N}_E(\lambda, \alpha) \cdot \overline{N}_E^T(\lambda, \alpha) \cdot d\lambda \qquad (3)$$

In (3), l is the axial length of the machine core, λ is a normalized coordinate mapping the whole airgap along the tangential direction by spanning in the [0,1) interval, $\mu_E(\lambda,\alpha)$ is the equivalent permeability function defined by (4) and $\overline{N}_E(\lambda,\alpha)$ is the vector containing the equivalent winding functions (EWFs) provided by (5).

$$\mu_E(\lambda, \alpha) = \mu_0 \cdot \frac{2 \cdot \pi \cdot r_G(\lambda, \alpha)}{\varepsilon_G(\lambda, \alpha)} \qquad (4)$$

$$\overline{N}_E(\lambda, \alpha) = \overline{N}(\lambda, \alpha) - \int_0^1 \left(\frac{\mu_E(\lambda, \alpha)}{\int_0^1 \mu_E(\lambda, \alpha) \cdot d\lambda} \right) \cdot \overline{N}(\lambda, \alpha)\, d\lambda \qquad (5)$$

The equivalent permeability function contains all the information regarding the anisotropies of the specific machine under analysis. In particular, these information are contained in the geometrical functions $r_G(\lambda,\alpha)$ and $\varepsilon_G(\lambda,\alpha)$ (see equation (4)), which represent the radius (distance from the geometrical axis) of the mean surface inside the main airgap and the equivalent magnetic thickness of the airgap, respectively; such functions may depend on the rotor position as well as on the location along the tangential direction. In (5), $\overline{N}(\lambda,\alpha)$ is the vector grouping the winding functions of all of the machine windings (generically named phases): each of them contains the information related to the distribution of the conductors of the corresponding phase among the different groups (slots), their location along the tangential direction and their orientation along the axial direction according to the reference direction assumed for the current flowing inside each phase.

Before going into the details of the quantities defined above and thus providing the inductances' waveforms with the implementation of (3), the damper cage modelling approach is described in the next section. The proposed model represents one of the main novelty of this work, as at the authors' knowledge has never been presented in the form shown below.

C. Circuital model of the damper cage

In general, the damper cage is composed of longitudinal bars located inside the poles which are wisely connected at the 2 end sides. Typically, the bars located inside each pole are connected by means of effective low-resistance end paths consisting in ring sectors or press-plates (as in the considered case study). Such groups of interconnected bars may be then connected each other by means of equally effective low-resistance paths, for example when a complete ring exists at each side. Alternatively, the different pole bar groups may be purposely left insulated, for example when the end rings are segmented and the bars are not in contact with, or may be connected by means of paths featuring a much higher resistance than the inter-bar connections. The cage type is labeled "complete" in the first case and "incomplete" in the second one.

When a complete cage is schematized as a set of b straight parallel bars connected by 2 circular end rings, its equivalent topology can be obtained by enlarging the front end ring and shifting it to the same plane of the rear end ring, in such a way to obtain a planar net as shown in Fig. 3.a. Such topology permits to conclude that the currents flowing in each side can be expressed as functions of the loop currents flowing in the natural loops obviously singled out in this planar representation, i.e. the b loops delimited by any couple of adjacent bars plus the inner loop corresponding to the rear end ring. With respect to the electromagnetic phenomena, the whole cage can be then modeled by leveraging again the general circuital approach illustrated in [11]: each loop can be considered as an equivalent short-circuited phase, meaning that the cage itself can be conceptually replaced with a set of closed conductive loops inside which the loop currents flow. Nevertheless, the resistive phenomena have also to be taken into account: for any bar or rear ring arc, the related voltage drop depends from both of the loop currents flowing in the 2 adjacent loops, meaning that a non-diagonal form of the resistance matrix has to be considered in the electric model.

When instead an incomplete cage is considered as in Fig. 3.b, the same approach above described may be used, but the number of natural loops is reduced to *b-2*p*, since the *2*p+1* loops connecting the facing bars located in adjacent pole groups are suppressed, as well as the rear end loop.

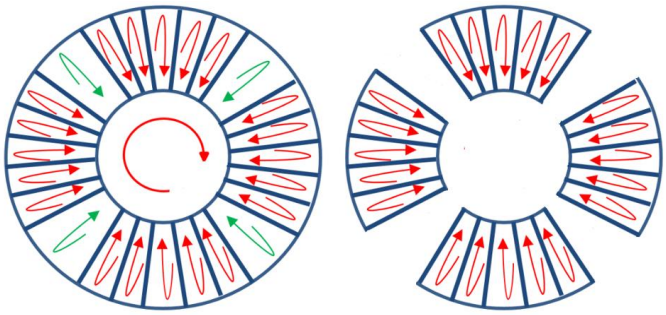

Fig.3. Equivalent circuit topology for a damper cage of "complete" (left) and "incomplete" type (right): example referred to the considered case study.

In any common SG, including the considered case study, typically the rotor poles are identical also for what concerns the deployment of the bars, usually featuring a symmetrical distribution with respect to the pole axis. Therefore, the physical symmetry related to the number of pole pairs *p* of the machine can be extended to the cage and also to the set of currents flowing in it, unless very unusual operating conditions are considered. This means that, at any given operative condition, the pattern of the currents flowing in the bars and end-rings inside any pole pair sector can be assumed to be identical in all of the other sectors, thus resulting in a reduced number of actually independent loop currents: *b/p+1* for complete cages, *b/p-2* for incomplete cages. Also, in case that also a full physical odd symmetry stands for the electromagnetic aspects according to the pole pitch, the current patterns related to the bars located in the 2 homologous sequences of poles may be assumed to be just opposite: the number of actually independent cage loop currents is then further reduced to *b/(2*p)+1* for complete cages and to *b/(2*p)-1* for incomplete cages.

The relationships above assumed among the correlated loop current patterns can be embedded in the model of the machine by assuming that the equivalent loop phases are properly connected in series/antiseries throughout the *2*p* poles of the machine, as shown in Fig. 4 for an incomplete cage. Such connection turns out convenient also for the imposition of the null voltage constraint to each short-circuited loop phase, since it is equivalently achieved by simply zeroing the total voltage across such compound phases thanks to the assumption of identical behavior.

For the considered case study, all of the hypotheses above assumed about the symmetry properties are verified, whereas the electrical connections between bar groups actually exist by means of paths along the press plates. However, these paths are much longer than the distance between adjacent bars, thus allowing for classifying the damper cage as "incomplete" at least as an acceptable approximation. According to Fig. 4 the number of compound phases used to represent the damper cage may be then reduced to 5, whereas the total number of phases in the machine is then 1+3+5=9: this is therefore the dimension of the vector differential equation shown in (1) that has to be solved in order to estimate the no-load voltage waveform, which is the main goal of this paper.

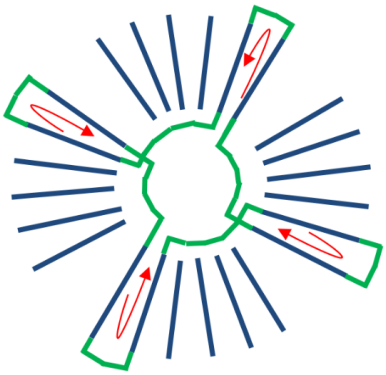

Fig.4. Compound planar schematic of a generic rotor cage loop for symmetrical machines.

A comparison between the WFs related to a single cage loop and to the compound phase incorporating the 4 cage loops located in corresponding positions along the rotor periphery is reported in Fig. 5. In general, any loop phase WF has obviously to be single-signed: this means that the corresponding equivalent WF calculated according to (5) will be a positive-negative square waveform (as shown in Fig. 5b), usually asymmetric, whatever is the trend of the equivalent permeability function. This in turn implies that the different loop phases will be magnetically coupled each other, besides being coupled to the field and armature windings.

On the other hand, in general the WF of the compound phase representing any set of corresponding loops features inherently an odd symmetry periodicity with respect to 1 pole pitch. Considering that the equivalent permeability function of any normal symmetric machine is either constant or features a period just equal to 1 pole pitch, it can be easily concluded that the equivalent WF will result just equal to the WF. This means that the equivalent WFs related to any couple of compound phases will not share any interval where both are non-zero, which implies that they result not magnetically coupled for what concerns the main flux tubes. Therefore, one can conclude that by using the compound phases not only the size of the system (1) is minimized, but also the complexity of the inductance matrix is reduced, thus reducing the computational burden.

D. Further considerations

Section II recalls the introductory aspects and the main functions of the generalised analytical model proposed by [11], valid for any electromagnetic device and properly adapted for the analysis of a 400*kVA* SG. However, updates regarding the effects of the stator slot openings (see Fig. 2) and an alternative way of modelling the damper cage (see Figures 4 and 5b) are proposed. All the assumptions above highlighted stand for machines provided with a symmetrical damper winding and

when normal operating conditions are considered. In fact, the hypothesis on the currents featuring opposite waveforms in corresponding bars of adjacent poles is always verified, unless any type of event resulting in an anomalous operation of the generator occurs. These include potential unbalances, single-phase operations, faults, etc. which basically produce an 'asymmetrical' response of the damping bars, thus not allowing to model the relevant winding as previously illustrated. However, all these events are not taken into consideration in this work, as the main goal is that of evaluating the no-load voltage waveform under normal 3-phase, symmetrical operation. To conclude up, the not-null elements of $L(\alpha)$ involving the rotor cage loops will be then evaluated by using the equivalent WFs of the type shown in Fig. 5b.

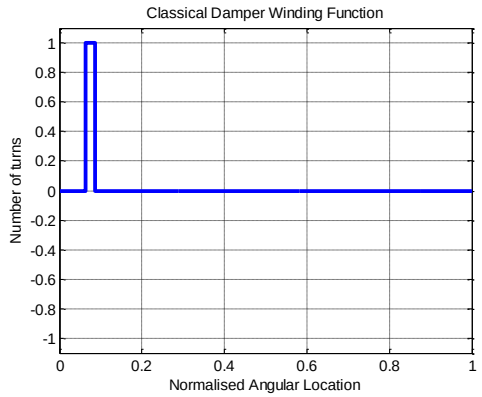

Fig. 5.a Winding function for 1 damper cage loop in the considered case study.

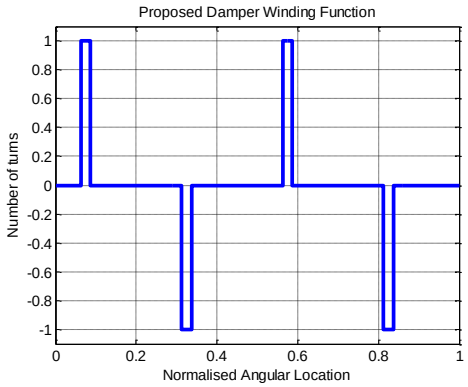

Fig.5.b Typical winding functions of damping cage loops: compound representation for symmetrical machines

III. The Hybrid Analytical-Numerical Approach

The implementation of the geometrical quantities shown in (4) and of the equivalent WFs provided by (5) allows for the calculation of the machine's inductances by means of (3). In this context, in order to set the concepts behind (4), the function $\mu_E(\lambda,\alpha)$ is shown in Fig. 6 at a specific, fixed rotor position. As salient-pole SGs exhibit an intrinsic symmetry that turns into a repetitive trend with period equal to $1/(2*p)$ for all the quantities involved in (4), $\mu_E(\lambda,\alpha)$ is plotted vs. λ inside 1 repetition period. Fig. 6 also highlights the effects of the slot openings and the rotor poles profile on the equivalent permeability function. The width and the depth of the dips that can be observed on such function are determined by a tuning procedure against the results obtained through the FE analysis of the SG being studied. In particular, the values of the characteristic parameters *a* and *b* (defined in Section II and shown in Fig. 2) of the slot opening are achieved by minimising the error, at any instant in time, between the no-load voltage waveform obtained by means of the proposed hybrid approach and that one determined through the corresponding FE model. The hybrid analytical-numerical model is described in this section, whereas the FE model and the comparison exercise will be provided in the following sections of this paper.

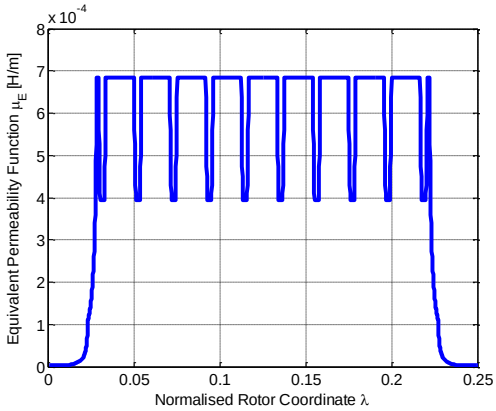

Fig. 6. Equivalent permeability function of the considered case study, after having applied the tuning procedure against the corresponding FE model.

A. The inductances

The inductances are calculated off-line as well as the approximated values of their derivatives with respect to the rotor position α. Having adopted the rotor coordinate λ for the definition of any function depending on the tangential location, it is worth highlighting that:

- The dependence on the position α of the self- and mutual-inductances related to the rotor circuits is exclusively due to the stator slot openings; this feature can be observed in Fig. 7, where the self-inductance of the field winding (first subplot), the mutual-inductance between the field winding and one of the rotor cage loop (second subplot) and the self-inductance of one cage loop (third subplot) are plotted against α.
- The dependence on the rotor position α of the stator self- and mutual-inductances, is due to the anisotropies featured by both the stator and rotor structures (slot openings and salient poles profile). This concept is shown in Figures 8 and 9. In particular the stator self- and mutual-inductances are shown in Fig 8. In Fig. 9, the mutual-inductances between the field winding (indicated as FW in the legend) and the 3 stator phases can be observed in the top subplot, while in the bottom one the mutual-inductances between one cage loop (indicated as CL in the legend) and the 3 stator windings are shown.

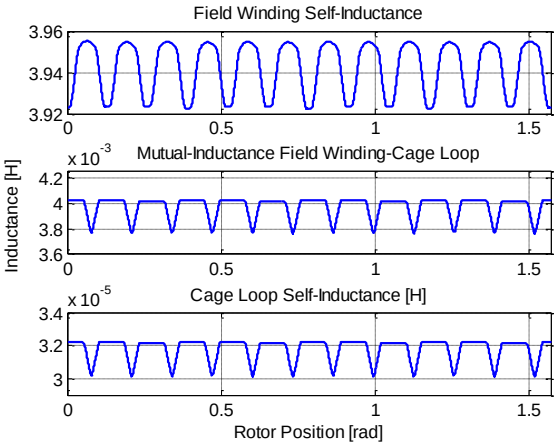

Fig. 7. Self- and mutual-inductances of the rotor circuits.

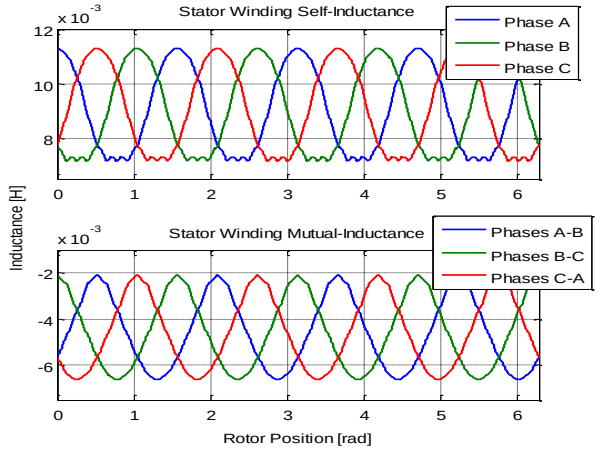

Fig. 8. Stator self- and mutual-inductances.

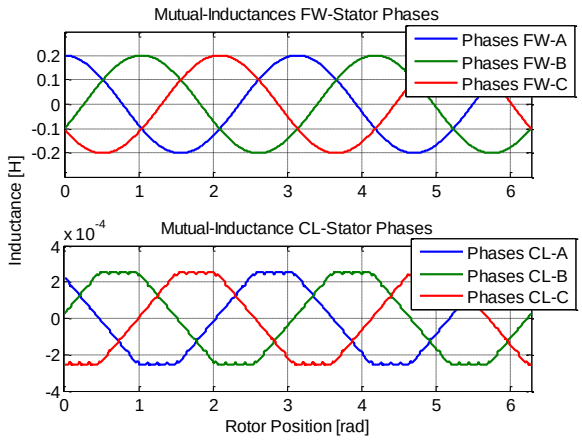

Fig. 9. Mutual-inductances between rotor and stator circuits.

When the inductance matrix $L(\alpha)$ is determined as well as the matrices $\partial L(\alpha)/\partial\alpha$ and R, it becomes possible to solve the system (1). Because of the induced nature of the damper cage currents, a numerical solution is needed to estimate such quantities. Hence, after being properly manipulated, (1) can be implemented in the Matlab-Simulink environment as shown in Fig. 10.

IV. Results and Comparison with FE Results

A. The numerical solution

In the schematic of Fig. 10, it can be observed that the voltage vector $\bar{v}(t)$ is used as input for the solution of system (1). Also, an additional term R_{add} can be seen in the model: this diagonal resistance matrix gives flexibility to the model as it allows to simulate different load conditions. For example, in order to simulate the no-load operation, all the terms contained in $\bar{v}$ are set to zero except for the term related to the field winding, while the terms in R_{add} inherent to the stator phases are set to a very large value practically ensuring that the stator currents will be almost null. Considering all this, it is now possible to obtain the no-load voltage waveform of the considered SG, as shown in Figures 12-14, where the results related to specific values of the excitation current are reported as examples.

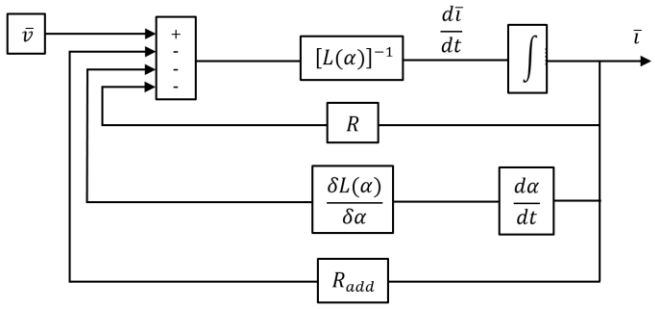

Fig. 10. General linear model of the electrical aspects implemented in Matlab-Simulink.

B. The FE model

A 2-D FE electromagnetic model of the SG analysed in this paper was get ready for validation purposes. The circuital part of the model permits to properly represent the connections of the circuits, whereas the damper bars are modelled as solid conductors to account for the skin effect. To be consistent with the assumption related to the linear behaviour of the ferromagnetic materials used for the stator and rotor cores, a high permeability magnetic steel is employed for the analysis. A transient with motion evaluation is then performed at no-load operation, with the field winding voltage imposed, the three-phase stator winding open-circuited (i.e. connected to a circuital resistance of a practical infinite value) and the damper bars connected in parallel.

C. Comparison of results

A comparison between the no-load waveforms provided by the analytical and FE methods is shown in Figures 12-14, for three different values of the excitation current. Those values are taken on the linear portion of the no-load characteristic of the considered generator, as the proposed hybrid model assumes the linear behaviour of the ferromagnetic materials. An experimental evaluation of the no-load curve for the

considered case study is shown in Fig. 11: the airgap line of the machine (in blue) can be also observed, highlighting that the saturation does not occur until the excitation current is below the 53% of the base field current, having defined the latter as that current value which provides the rated voltage when the armature phases are open-circuited. An excellent similarity between the no-load phase voltage waveforms can be observed in all the cases, proving the validity of the mixed analytical-numerical approach. However, although the proposed model is based on the assumption of linear behaviour of the ferromagnetic materials, it is interesting to observe the deviations of the waveforms obtained through the implemented model from those evaluated by a FE analysis, when in the relevant model non-linear materials are employed. Fig. 15 shows this additional comparative exercise, where a value equal to the 29% of the base field current is used (as for the evaluation of the waveforms of Fig. 13). Although a good match can still be observed between the no-load waveforms of Fig. 15, small discrepancies can be observed due to additional peaks introduced by the non-linear materials, when these are implemented in the FE model for the stator and rotor cores of the considered machine.

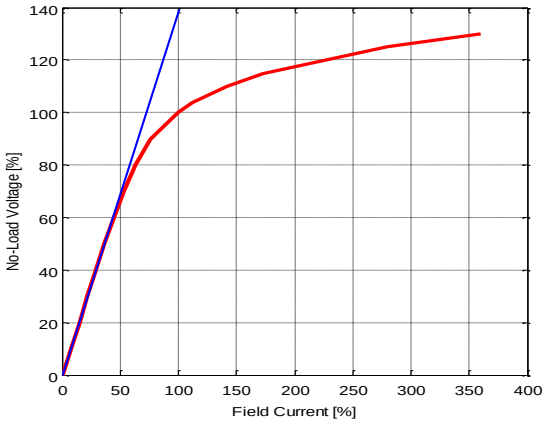

Fig. 14. Experimental no-load characteristic of the considered generator

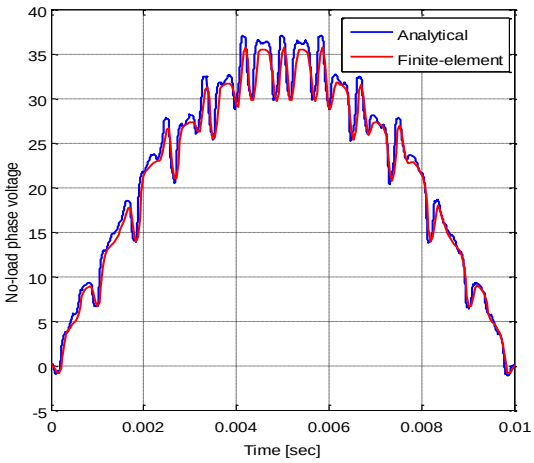

Fig. 12. No-load voltage waveforms: analytical vs. FE results at 7.5% of the base field current.

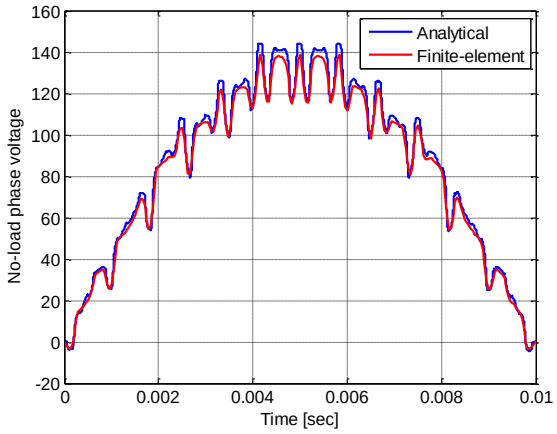

Fig. 13. No-load voltage waveforms: analytical vs. FE results at 29% of the base field current.

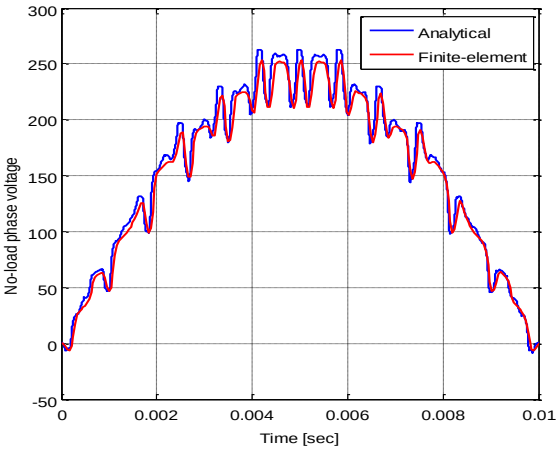

Fig. 14. No-load voltage waveforms: analytical vs. FE results – at 53% of the base field current.

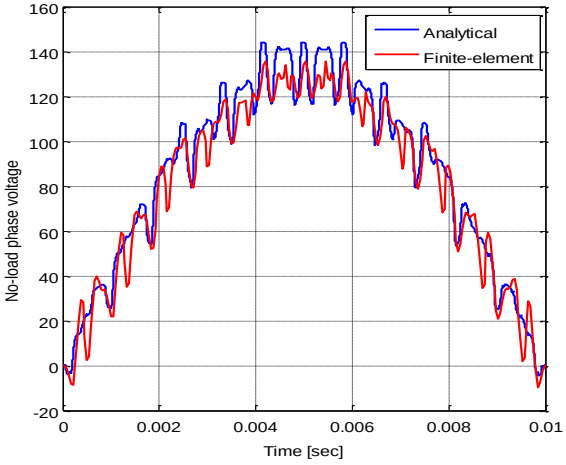

Fig. 15. No-load voltage waveforms: analytical vs. FE results with non-linear materials – at 29% of the base field current.

V. CONCLUSIONS

This paper aims at accurately estimating the no-load voltage waveform in a particular salient-pole SG, when operating in linear condition, by implementing a mixed analytical-numerical model that turns out much faster than the classic FE method. Focus was given to the damper cage analysis, whose modelling was carried out in an alternative way compared to the classical literature: this allowed to drastically reduce the number of equations to be solved. Promising results have been achieved at different no-load operating points, showing the validity of the proposed hybrid methodology. The analytical results have been compared to the FE ones, also when a non-linear material is employed for the corresponding analysis. This showed some limitations of the proposed approach, although the similarity between results was however very good.

Considering the above, further work is on-going aiming to include in the model the most representative non-linear parts of the machine in order to better simulate the machine operation also on-load.

REFERENCES

[1] S.Nuzzo, M.Galea, C. Gerada, D. Gerada, A. Mebarki, N. L. Brown, "Damper cage loss reduction and no-load voltage THD improvements in salient-pole synchronous generators", 8th IET International Conference on Power Electronics, Machines and Drives (PEMD 2016), pp.1-7, 2016.

[2] G. Klempner, I. Kerszenbaum, "Handbook of Large Turbo-Generator Operation and Maintanance", Wiley-IEEE Press, 2008.

[3] G. Traxler-Samek, T. Lugand, A. Schwery, "Additional losses in the damper winding of large hydrogenerators at open-circuit and load conditions", IEEE Trans. Ind. Electron., vol. 57, no. 1, pp. 154-160, Jan. 2010.

[4] S. Nuzzo, M. Degano, M. Galea, C. Gerada, D. Gerada, N. L. Brown, "Improved damper cage design for salient-pole synchronous generators," IEEE Trans. Ind. Electron., vol. 64, no. 3, pp. 1958-1970, 2017.

[5] M. M. Liwshitz, "Harmonics of the salient pole synchronous machine and their effects part III. Differential leakage of the damper winding with respect ot the main wave. Current distribution in the damper bars," Trans. Amer. Instr. Elect. Eng. Power App. Syst., Part III, vol. 77, no. 3, pp. 462-469, Apr. 1958.

[6] A. Tessarolo, C. Bassi, D. Giulivo, "Time-stepping finite-element analysis of a 14-MVA salient-pole shipboard for different damper winding design solution," IEEE Trans. Ind. Electron., vol. 59, no. 6, pp. 2524-2535, Jun. 2012.

[7] H. Karmaker, A.M. Knight, "Investigation and simulation of fields in large salient-pole synchronous machines with skewed stator slots," IEEE Trans. Energy Convers., vol. 20, no. 3, pp. 604-610, Sep. 2005.

[8] A.M. Knight, H. Karmaker, K. Weeber, "Use of a permeance model to predict force harmonic components and damper winding effects in salient-pole synchronous machines," IEEE Trans. Energy Convers., vol. 17, no. 4, pp. 709-716, Dec. 2002.

[9] E. Wallin, M. Ranlof, U. Lundin, "Design and construction of a synchronous generator test set-up," presented at the Int. Conf. Electrical Machines (ICEM), Rome, Italy, Sep. 6-8, 2010, Paper RF-008982.

[10] G. Traxler-Samek, T. Zickermann, A. Schwery, "Cooling airflow, losses and temperatures in large air-cooled synchronous generators", IEEE Trans. Ind. Electron., vol. 57, no. 1, pp. 172-180, Jan. 2010.

[11] P. Bolognesi, "A mid-complexity analysis of lung-drum-type electric machines suitable for circuital modelling," in Proc. ICEM 2008 Conf., paper no. 99.